Micro-Ellipso-Height-Profilometry

K. Leonhardt, H.-J. Jordan and H.J. Tiziani
Institut für Technische Optik, Pfaffenwaldring 9, 7000 Stuttgart 80, Germany

Received 27 August 1990

A new instrumental concept for surface measurement is described. In Micro-Ellipso-Height-Profilometry three independent profiles $h(x)$, $\Psi(x)$ and $\Delta(x)$ of a surface are measured from one diffraction limited scanning spot. The basic equations for the extraction of these three quantities are derived and first results are discussed.

1. Introduction

With optical profilometers the profilometric height $h(x)$ of rough or structured surfaces is measured. However, they cannot determine the optical constants or ellipsometric data. On the other hand, ellipsometers can measure the ellipsometric angles Δ and Ψ of smooth surfaces with vanishing roughness, but they cannot supply the structure- and roughness-information given by the profilometric height $h(x)$.

The Micro-Ellipso-Height-Profilometer MEHP measures three independent quantities $h(x)$, $\Delta(x)$ and $\Psi(x)$ from one single diffraction limited scanning spot. Combined changes in the height and in the material, contaminations, oxidations or changes in the thickness of thin films etc. can be detected unambiguously.

As an example, the true height of a step on the surface accompanied with a change in the material cannot be measured directly with interferometry and profilometry, because of the phase change associated with the change in material. It can be determined unambiguously with MEHP from the combined information of $h(x)$, $\Delta(x)$, and $\Psi(x)$.

2. Principle of the Micro-Ellipso-Height-Profilometer

Fig. 1 shows a schematic diagram of the MEHP. A polarizing beamsplitter PBS, a quarterwave plate QWP_{diag}, an electro optic modulator EOM and a high numerical aperture microscope objective MO are transmitted by the gaussian beam of a laser at an off-axis displacement e. The gaussian beam with the waist diameter $w_f \ll D$ (D is the diameter of the aperture of the objective) is focused onto the surface. The microscope objective (100×0.9 POL) must be selected to be appropriate for polarization applications. Due to the displacement e the beam axis of the probing beam subtends an angle φ_0 in the object space. This is the ellipsometric angle of incidence. In our first realization φ_0 was chosen to be 45°.

After the reflection at the surface the beam passes again the microscope objective MO, the electrooptic modulator EOM and the quarterwave plate QWP_{diag}. The s-polarized component of the polarization ellipse is reflected by the polarizing beamsplitter PBS and enters the detection system for the measurement of the profile-height and the ellipsometric angles.

For ellipsometric information the intensity of the beam 'a' at the CCD-array is measured as a function of the applied voltage U_p to the EOM. For this intensity measurement the signal of the pixels which are illuminated by beam 'a' is summed up. The detection of the profile height $h(x)$ is described in section 4.

3. Theory of the ellipsometric measurement

The polarization transforming components can be described by their Jones matrices [1,2]. Ideal and nondepolarizing components and isotropic surfaces

0030-4018/91/$03.50

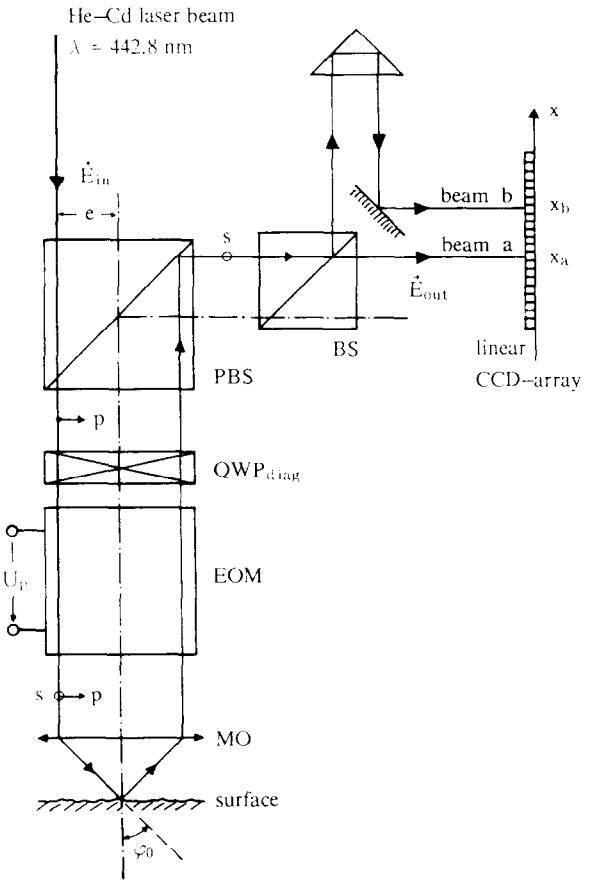

Fig. 1. Optical system layout of the MEHP.

are assumed. The Jones vector of the incoming light is $\boldsymbol{E}_{in}$, the Jones vector after reflection on the PBS is $\boldsymbol{E}_{out}$ (fig. 1),

$$\boldsymbol{E}_{out} = \overline{\overline{T_{PBS}}}\ \overline{\overline{L_{-45^\circ}}}\ \overline{\overline{EOM}}\ \overline{\overline{OBJ}}\ \overline{\overline{L_{45^\circ}}}\ \overline{\overline{T_{PBS}}}\ \boldsymbol{E}_{in}\,, \tag{1}$$

with

$$\overline{\overline{T_{PBS}}} = \begin{bmatrix} 1 & 0 \\ 0 & 0 \end{bmatrix} \quad \text{PBS, transmission}\,, \tag{2}$$

$$\overline{\overline{R_{PBS}}} = \begin{bmatrix} 0 & 0 \\ 0 & 1 \end{bmatrix} \quad \text{PBS, reflection}\,, \tag{3}$$

$$\overline{\overline{L_{45^\circ}}} = \frac{1}{\sqrt{2}}\begin{bmatrix} 1 & \mathrm{i} \\ \mathrm{i} & 1 \end{bmatrix} \quad \text{QWP, fast axis } +45^\circ\,, \tag{4}$$

$$\overline{\overline{L_{-45^\circ}}} = \frac{1}{\sqrt{2}}\begin{bmatrix} 1 & -\mathrm{i} \\ -\mathrm{i} & 1 \end{bmatrix} \quad \text{QWP, fast axis } -45^\circ\,, \tag{5}$$

$$\overline{\overline{EOM}} = \frac{1}{\sqrt{2}}\begin{bmatrix} \exp(-\mathrm{i}\phi & 0 \\ 0 & \exp(+\mathrm{i}\phi) \end{bmatrix} \quad \text{EOM}\,, \tag{6}$$

$$\overline{\overline{OBJ}} = \begin{bmatrix} m_1 & 0 \\ 0 & m_2 \end{bmatrix} \quad \text{Object matrix}\,. \tag{7}$$

The complex coefficients m_1 and m_2 of the reflection on the object surface contain the ellipsometric information. For a simple boundary between two media they are given by Fresnel formulae [3].

The phase in the matrix elements of the EOM is given by

$$\phi = \tfrac{1}{4}\pi\, U_p / U_{\lambda/4}\,, \tag{8}$$

with U_p the voltage applied to the EOM and $U_{\lambda/4}$ the voltage of quarterwave retardation between the Jones vectors of the p- and the s-polarisation. The axis of the EOM were parallel to the ps-coordinate system.

The ellipsometric angles Δ and Ψ are defined by [4]

$$\tan\Psi = |m_2|/|m_1|\,, \quad 0 \leqslant \Psi \leqslant 90^\circ\,, \tag{9}$$

$$\Delta = \arg(m_2 - m_1)\,, \quad 0 \leqslant \Delta \leqslant 180^\circ\,. \tag{10}$$

The intensity I_{out} of the light entering the detection system is given by [1,2]

$$I_{out} = \boldsymbol{E}^*_{out}\boldsymbol{E}_{out}\,. \tag{11}$$

With eqs. (2) to (7) and eq. (11) we find

$$I_{out} = \tfrac{1}{4}\{|m_1|^2 + |m_2|^2 - 2|m_1||m_2|\cos[4\phi + \arg(m_2 - m_1)]\}\,. \tag{12}$$

This intensity is measured as a function of the voltage U_p applied to the EOM. $I_{out}(U_p, m_1, m_2)$ as shown in fig. 2 has maxima I_{max} and minima I_{min} according to

$$I_{max/min} = |m_1|^2 + |m_2|^2 + / - 2|m_1||m_2|\,. \tag{13}$$

The visibility V is defined by

$$V = (I_{max} - I_{min})/(I_{max} + I_{min})\,, \quad 0 \leqslant V \leqslant 1\,. \tag{14}$$

With eq. (13) the visibility leads to

$$V = 2\frac{|m_1||m_2|}{|m_1|^2 + |m_2|^2} = \frac{2\tan\Psi}{1 + \tan^2\Psi}, \tag{15}$$

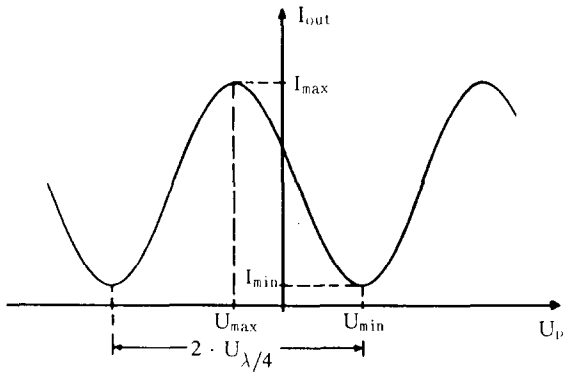

Fig. 2. The intensity I_{out} versus EOM voltage U_p.

and therefore, the ellipsometric angle Ψ is

$$\Psi=\arctan[(1/V)(1-\sqrt{1-V^2})]\,. \tag{16}$$

In order to derive the ellipsometric angle Δ we consider the voltages U_{max} and U_{min} leading to the maxima and minima of the intensity I_{out}.

For I_{max}, from the argument of the cosine in eq. (12) we find

$$\pi\, U_{max}/U_{\lambda/4}+\Delta=\pm\pi\,, \tag{17}$$

and for I_{min} we find

$$\pi\, U_{min}/U_{\lambda/4}-\Delta=0\,. \tag{18}$$

From eq. (17) and eq. (18), Δ can be calculated as

$$\Delta=\tfrac{1}{2}\pi[1-(U_{max}-U_{min})/U_{\lambda/4}]\,. \tag{19}$$

4. Determination of the profilometric height *h(x)*

The measurement of the topographic height $h(x)$ is based on microtriangulation. The profile is calculated from the beam coordinates, obtained by the CCD-array (fig. 1). For the evaluation of the height no voltage is applied to the EOM.

The topography of the surface can be described by two parameters, the profile height $h(x)$ and the surface slope $\alpha(x)$. The focal plane in the object space shall be identified with the profile height $h=0$ (fig. 3). For a reflecting surface element with a height $h(x)$, reflection takes place at an off-axis position x_1 in the object space. The surface slope $\alpha(x)$ causes a

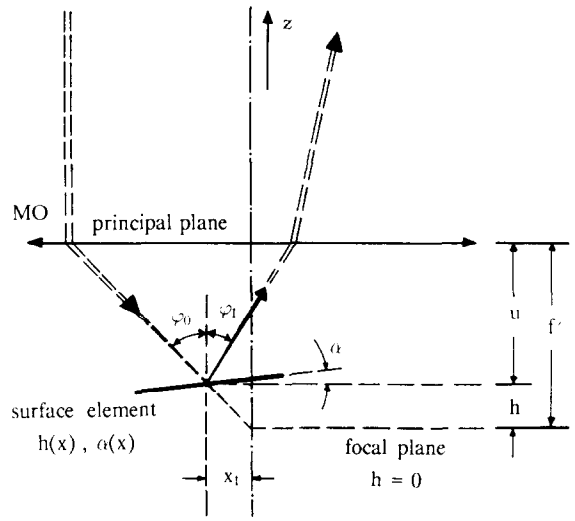

Fig. 3. Schematic diagram showing the relevant quantities of the reflecting surface element and the parameters of the reflected beam.

deviation of the direction of the beam after reflection. This modified direction is φ_1.

In the special case $h(x)=0$ and $\alpha(x)=0$, reflection takes place at an surface element perpendicular to the optical axis and located in the focal plane of the microscope objective. Then, after passage through the objective, the beam in the image space is displaced parallel to the optical axis by e.

In the general case $h(x)\neq 0$ and $\alpha(x)\neq 0$, the beam in the image space is not parallel to the optical axis. The direction of the beam and his position in the image space depend on the parameters x_1 and φ_1 of the beam in the object space.

The ray trace after the reflection at the surface can be calculated by the method of the ray transfer matrices (*ABCD*-matrices) [5,6],

$$\begin{bmatrix} x_a \\ \eta_a \end{bmatrix}=\begin{vmatrix} A & B \\ C & D \end{vmatrix}\begin{bmatrix} x_1 \\ \eta_1 \end{bmatrix}. \tag{20}$$

The quantities η_i are the directional derivatives of the coordinates x_i, with respect to the optical axis (z-direction),

$$\eta_i=\mathrm{d}x_i/\mathrm{d}z=\tan\varphi_i\,. \tag{21}$$

The output quantities x_a and η_a are the beam parameters in the plane of the CCD-array. They are lin-

early dependent on the input quantities x_1 and η_1. Therefore, x_a and η_a together contain the full information of the two surface parameters $h(x)$ and $\alpha(x)$.

Consider the beam a (fig. 1) on his way from the surface to the CCD-array. The *ABCD*-matrix of the MEHP for this beam is composed of three fundamental matrices, as described in refs. [5,6]. In the sequence of acting on the beam these matrices are

$$\overline{\overline{M_u}}=\begin{vmatrix}1 & u\\ 0 & 1\end{vmatrix},\quad \overline{\overline{M_{mo}}}=\begin{vmatrix}1 & 0\\ -1/f' & 1\end{vmatrix},\quad \overline{\overline{M_s}}=\begin{vmatrix}1 & s_a\\ 0 & 1\end{vmatrix}. \tag{22}$$

$\overline{\overline{M_u}}$ is the *ABCD*-matrix for the transfer over the distance u from the reflecting surface element to the principal plane of the microscope objective; $\overline{\overline{M_{mo}}}$ is the matrix for a thin lens of focal length f' and $\overline{\overline{M_s}}$ is the matrix for the transfer over distance s_a from the principal plane of the microscope objective to the CCD-array.

The input parameters x_1 and η_1 (φ_1) are related to the parameters h and α of the topography (fig. 3),

$$x_1 = h\tan\varphi_0 = (f'-u)\tan\varphi_0\,, \tag{23}$$

$$\eta_1 = \tan\varphi_1 = \tan(2\alpha-\varphi_0)\,. \tag{24}$$

The output parameters of the beam 'a' at the CCD-array are

$$\begin{bmatrix}x_a\\ \eta_a\end{bmatrix} = \overline{\overline{M_s}}\,\overline{\overline{M_{mo}}}\,\overline{\overline{M_u}}\begin{bmatrix}x_1\\ \eta_1\end{bmatrix} = \begin{vmatrix}1-s_a/f' & u+s_a(1-u/f')\\ -1/f' & 1-u/f'\end{vmatrix}\begin{bmatrix}(f'-u)\tan\varphi_0\\ \tan(2\alpha-\varphi_0)\end{bmatrix}. \tag{25}$$

The slope η_a of the beam (with respect to the optical axis) cannot be measured by the CCD-array. Only eq. (26a) for the coordinate x_a is applicable.

In order to obtain the second equation for the elimination of the surface slope α, we split the beam by the beamsplitter BS into two beams a and b (fig. 1),

$$x_{a,b} = (1-s_{a,b}/f')\,(f'-u)\tan\varphi_0 + [u+s_{a,b}(1-u/f')]\tan(2\alpha-\varphi_0)\,. \tag{26a,b}$$

The coordinates x_a and x_b of the two beams at the CCD-array are measured both with respect to their individual optical axes. With s_a and s_b known, the surface slope $\alpha(x)$ can be eliminated from the two eqs. (26a,b). This leads to

$$h = f'\left[1-\frac{m}{(x_a-x_b)+m}\right]. \tag{27}$$

The factor m is given by

$$m = (s_b-s_a)\tan\varphi_0 + (1/f')(x_b s_a - x_a s_b)\,. \tag{28}$$

Eq. (27) gives the measured profile height $h(x)$, which is independent of defective influences of the surface slope.

The distances s_q (q=a,b) can be obtained from the derivative of x_q in eq. (26q) to the distance u ($=f'-h$) with $\alpha=0$,

$$s_q = f'\left[\frac{1}{2\tan\varphi_0}\left.\frac{\mathrm{d}x_q}{\mathrm{d}u}\right|_{\alpha=0}+1\right]. \tag{29}$$

The distance s_b we have chosen to be $s_b \approx 2s_a$.

5. Results

On polished surfaces a height resolution of $\delta h \approx 4$ nm for a range of $h_{tot} \approx 8000$ nm was obtained. The Ψ-resolution was $\delta\Psi \approx 0.2°$ and the Δ-resolution was $\delta\Delta \approx 0.4°$. The lateral resolution is given by the diffraction limited scanning spot as $\delta x_{lat} \approx 3$ μm. Measuring time was $t \approx 3$ s for the complete data acquisition of one scanning point. The scanning speed can be essentially improved by faster hardware and optimized software.

A typical trace obtained by the MEHP from a surface with a change in material is shown in fig. 4. A bar of aluminium-alloy and a bar of technical copper were mounted adjacent to each other, machined plane, and roughly polished on a metallographic polishing disk (fig. 4a). The profile of the height $h(x)$ (fig. 4b) shows microroughness due to imperfect polishing, which is clearly resolved, superposed by runout errors of the scanning stage. The microroughness of the aluminium surface is shown to be larger than that of the copper. Also the height variation induced by the polishing process due to the different hardnesses is clearly revealed. Due to the good lateral resolution, the profile shows a distinctive indent at the junction between the bars.

The profile of the ellipsometric angle $\Psi(x)$ is

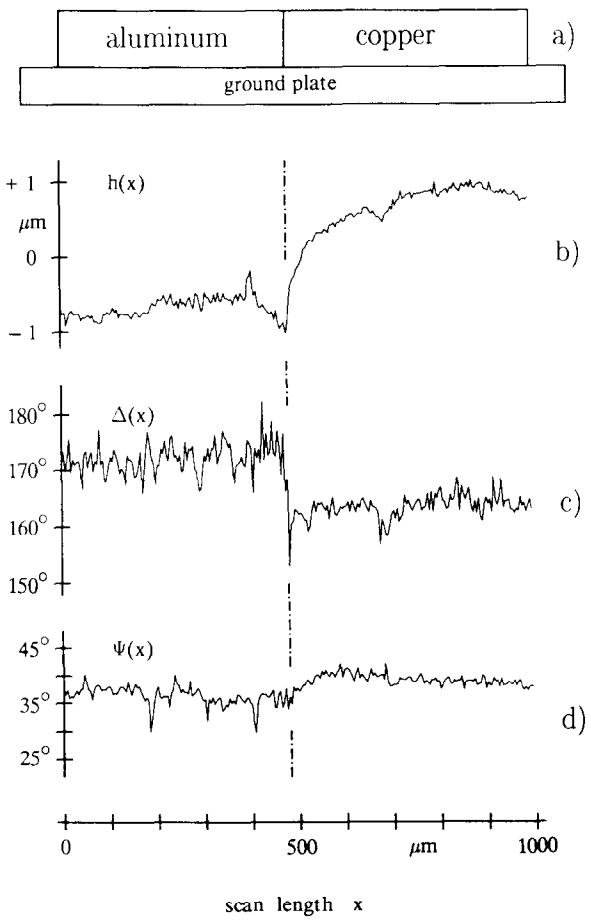

Fig. 4. The aluminum-copper specimen in a schematic drawing (a), the height profile $h(x)$ (b) and the profiles of the appropriated ellipsometric angles $\Delta(x)$ (c) and $\Psi(x)$ (d).

shown in fig. 4d. At $\lambda = 442.8$ nm, the calculated Ψ-values of aluminium and copper are nearly equal and only a small discontinuity is to be expected. However, the microstructure of $\Psi(x)$ as shown by fig. 4d, is not due to random noise; the measurement could be repeated with good reproducibility.

In the $\Delta(x)$-profile (fig. 4c) a pronounced discontinuity at the junction is measured. This demonstrates the capability of MEHP to discriminate between different materials. A valuable feature of the MEHP is that the $\Delta(x)$-variations are not affected by the height variations.

6. Conclusion

From the principle arrangement in fig. 1 it can be seen, that a MEHP can be constructed as a compact and robust sensor. Ellipsometric data acquisition is done electro-optically, by use of a Pockels cell, without rotating polarizers or analysers, as in conventional ellipsometry. The presented method for the analysis of the topography of the surface is independent from local surface slopes.

The combined information from the $h(x)$-, $\Delta(x)$- and $\Psi(x)$-profiles with high lateral resolution, excellent spatial allocation and mutual independence of the different profiles can lead to an unambiguous determination of structured surfaces and film systems.

Acknowledgement

This work was supported by "Deutsche Forschungsgemeinschaft DFG" under "DFG Ti 119/9-1".

References

[1] W.A. Shurcliff, Polarized light (Harvard University Press, Cambridge, MA 1962).
[2] K. Leonhardt, Optische Interferenzen (Wissenschaftliche Verlagsgesellschaft, Stuttgart, 1981).
[3] M. Born and E. Wolf, Principles of optics, 5th edition (Pergamon Press, Oxford, 1975).
[4] R.M.A. Azzam and N.M. Bashara, Ellipsometry and polarized light (North-Holland, Amsterdam, 1977).
[5] H. Kogelnik and T. Li, Appl. Optics 5 (1966) 1550.
[6] A.E. Siegman, Lasers (University Science Books, Oxford, 1986).